A Model for Predicting Fracture Toughness in Overaged 7000 Alloy Forgings

Maja Vratnica[1,a], Zorica Cvijović[2,b], Marko Rakin[2,c] and Ivana Cvijović[3,d]

[1] Faculty of Metallurgy and Technology, University of Montenegro,Cetinjski put b.b., 81000 Podgorica, Montenegro

[2] Faculty of Technology and Metallurgy, University of Belgrade, Karnegijeva 4, 11120 Belgrade, Serbia

[3] Institute of Nuclear Sciences "Vinča", P.O. Box 522, 11001 Belgrade, Serbia

[a]majav@cg.ac.yu, [b]zocvij@tmf.bg.ac.yu, [c]marko@tmf.bg.ac.yu, [d]ivanac@vin.bg.ac.yu

Keywords: 7000 series alloys, Overaged forgings, Fracture toughness, Microstructural parameters, Fracture modes, Micromechanical model.

Abstract. An attempt to develop a multiple micromechanism-based model for predicting plane-strain fracture toughness, K_{Ic}, of overaged 7000 alloy forgings has been made. The proposed model reveals the quantitative relations between the fracture toughness, fraction of the main fracture modes and parameters such as volume fraction, size and density of differently sized second-phase particles and precipitate-free zones. The new model is validated by the present quantitative data of microstructural and fractographic analysis performed along with mechanical tests on hot-forged plates subjected to the T73 temper. The relative parameters changed by the compositional variations were determined in the R-L and L-R orientations. It was found that the predicted K_{Ic} values well represent the tendency of fracture toughness change. The new model provides better agreement for the case of dominant transgranular fracture mode represented in the R-L orientation.

Introduction

The critical fracture toughness properties of the high-strength 7000 series Al-Zn-Mg-Cu alloys limit their application in the highly stressed region [1,2]. The microstructural inhomogeneity mainly associated with the existence of differently sized second-phase particles plays very important role in triggering the fracture process and then in determining the fracture toughness level [1,3,4]. Commercial precipitation-hardened alloys have a complex microstructure, which typically consists of coarse intermetallic (IM) particles with sizes in the range of 1 to 20 μm, intermediate Cr-, Mn- or Zr-rich dispersoids having 0.05- to 0.5- μm average size, relatively coarse quench-induced precipitates and fine strengthening precipitates being smaller than 0.02 μm [5]. Thus, the sizes of the second-phase particles span a length scale of over three orders of magnitude.

All these types of second-phase particles make a significant positive or negative contribution to the mechanical properties of aged 7000 alloys [1,5]. The coarse IM particles are detrimental to their ductility and fracture toughness. They fracture or separate from the matrix under service loading, acting as crack initiators or preferential crack paths. A primary voiding at coarse IM particles is, therefore, an important fracture mode in these alloys. The smaller dispersoids used for avoiding recrystallisation are more resistant to cracking or decohesion than are the coarse IM particles, providing sites for ductile void growth. The increase in ageing precipitates can reduce fracture resistance, because these precipitates are the major contributors to the strength of alloys. However, their relative contribution to the overall fracture depends on their coherency, size and spacing in the matrix. Hence, the transgranular fracture is controlled by the precipitation state. In addition, a yield stress and work hardening rate in the grain interior after heat treatment affect the plastic behaviour of the grain boundary vicinity, *i.e.*, the precipitate-free zones (PFZs) adjacent to the high angle boundaries and indirectly influence the intergranular ductile fracture in the PFZs. The fracture of the grain boundary in the PFZs is also coupled with the presence of coarse and closely spaced grain

boundary precipitates and PFZs width of the order of μm. The PFZs, much softer than grain interior, promote easier crack propagation within them and intergranular fracture.

Consequently, the various fracture modes are simultaneously present. In order to quantitatively understand how the multiscale microstructural features exert coupling effects on the fracture properties, it is necessary to bring a micromechanical model, which is enable to predict the fracture toughness when several fracture modes influenced by microstructural parameters associated with every population of second-phase particles coexist. The purpose of the present study is to develop such a model for predicting plane-strain fracture toughness, K_{Ic}, of the overaged 7000 alloys in the form of thick plate products, which are important as different parts of an aircraft. Insight into the fracture micromechanisms was obtained by varying the microstructure through alloy composition.

Experimental Procedure

Three commercial alloys belonging to the group of maximal alloying with the compositions (in mass %): Al-7.45Zn-2.47Mg-1.53Cu-0.25Mn-0.17Cr-0.15Zr-0.11Si-0.12Fe (Alloy 1), Al-7.30Zn-2.26Mg-1.55Cu-0.29Mn-0.18Cr-0.13Zr-0.09Si-0.16Fe (Alloy 2) and Al-7.65Zn-2.26Mg-1.55Cu-0.25Mn-0.18Cr-0.11Zr-0.11Si-0.26Fe (Alloy 3) were supplied as uniaxially hot-forged 50-mm-thick pancake-type plates subjected to the T73 heat treatment including solution treating at 460^{o}C for 1h, water quenching and ageing at 100^{o}C and 160^{o}C for 5h. The difference in microstructural attributes associated with the coarse IM particles and precipitates was obtained by different contents of Zn and Mg alloyed for precipitation hardening and total (Fe+Si) impurity content.

Plane-strain fracture-toughness tests were carried out in accordance with ASTM E399. The single-edge-notched three-point bending (SEB) specimens were tested in the R-L orientation. The values of K_{Ic} were determined from the J-integral data. The J-integral and crack growth, Δa, were calculated in accordance with ASTM E1152 and ASTM E813. Compact-tension (CT) specimens were used to determine the K_{Ic} for a critical L-R orientation. All specimens were fatigue precracked according to ASTM standard specifications. Tensile tests were performed on the corresponding R and L orientation specimens in accordance with ASTM E8-95.

The microstructures of overaged plates were examined using a Reichert-Jung MeF3 light microscope (LM), the secondary electron mode of a Philips XL30 scanning electron microscope (SEM) operating at 20 kV and a Technai F20S-Twin transmission electron microscope (TEM) with a field emission gun. The coarse particles type was determined by a selective etching and energy-dispersive X-ray spectroscopy (EDS) analysis performed on the SEM. The volume fraction, f_v, of coarse IM particles and resolved intragranular precipitates, their size expressed by the average intercept length, L, or average diameter, d, the coarse IM particles spacing, λ, and the PFZs width, w_{PFZs}, were estimated by means of image analyzer operating on the LM. The identification of various precipitates was performed using EDS system attached to the TEM. The SEM fractographic analysis were also performed in order to identify the fracture micromechanisms in the central plane-strain region of the plastic zone. The contributions of individual fracture modes to the overall fracture were quantitatively assessed by measuring the surface area fraction, A_A, on a large number of the SEM fractographs.

Results and Discussion

Microstructural Characterisation. All three overaged plates have very similar microstructures comprised of a large pancake-shaped grains elongated in direction of prevailing deformation and significant amount of second-phase particles, which can be classified in the five groups (Fig. 1).

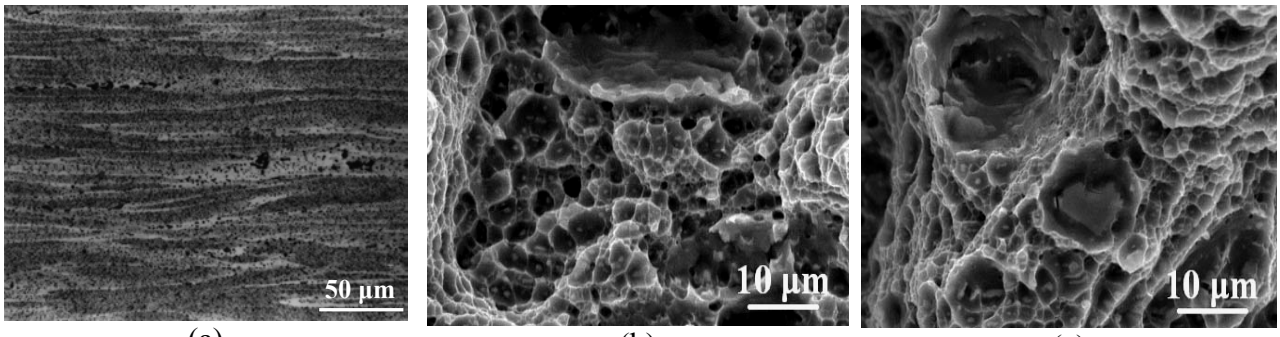

(a) (b) (c)

Fig. 1. LM micrograph of alloy 2 (a) and SEM fractographs of alloy 2 (b), (c).

Coarse IM particles with average size from 1.27 to 2.43 µm are inhomogeneously distributed at grain and dendrite arm boundaries. They are linearly arranged in the C direction, which is consistent with the applied forging process. Most of these particles are unsoluble Fe-rich phases. They are mainly of two kinds: $(Cu,Fe,Mn)Al_3$ (Fig. 2a) and Al_7Cu_2Fe (Fig. 2b). As the Fe content increases, their volume fraction and size increase while spacing decreases (see Table 1). Since the larger particles crack more often, these particles having 1.99- to 2.43- µm average size and lower fracture strength than those of other phases [6] should be more detrimental for damage evolution and fracture toughness. The soluble η-$Mg(Zn,Cu,Al)_2$ (Fig. 2d), S-$CuMgAl_2$ (Fig. 2e) and Mg_2Si (Fig. 2c) phases are not present in a large amounts. As can be seen from Table 1, alloy 1 with the highest (Zn+Mg) content shows their maximum fraction which is less than 0.29 vol.%. The dominant undissolved phase is based on the Mg_2Si. Although the Mg_2Si particles with average size from 1.70 to 2.09 µm are not present in much higher amount, they are larger than those of η and S phases, so that could show a much greater influence on the fracture processes. The presence of coarse η and S particles, containing alloying elements, after homogenisation and solution treatment indicates that Zn and Mg do not have the same potential to influence precipitation behaviour of the alloys.

Table 1. Geometrical parameters of investigated forgings as a function of orientation.

Alloy	*Specimen orientation*	*Coarse IM particles*									w_{PFZs} [µm]
		η + S			*Mg_2Si*			*Fe-rich **			
		f_v [vol.%]	*L* [µm]	λ [µm]	f_v [vol.%]	*L* [µm]	λ [µm]	f_v [vol.%]	*L* [µm]	λ [µm]	
1	R-L	0.147	1.56	1055	0.144	1.94	1350	0.236	2.08	878	1.87
	L-R	0.159	1.63	1025	0.125	1.74	1394	0.227	2.00	883	1.47
2	R-L	0.095	1.27	1334	0.134	1.92	1425	0.440	2.06	465	2.14
	L-R	0.048	1.29	2686	0.094	1.70	1807	0.357	1.99	537	1.56
3	R-L	0.046	1.38	3031	0.146	2.09	1435	0.532	2.37	444	1.90
	L-R	0.119	1.63	1363	0.147	1.95	1319	0.590	2.43	410	1.37

* Fe-rich phases = $(Cu,Fe,Mn)Al_3$ + Al_7Cu_2Fe

The second type of particles visible under the LM is round intragranular η-$Mg(Zn,Cu,Al)_2$ precipitates with average diameter of ~ 0.55 µm, which appear during homogenisation and are partly transformed in S-$CuMgAl_2$ particles during solute treatment (Fig. 3a). Due to the higher amount of the Zn and Mg dissolved in the matrix, their volume fraction is much greater in alloys 2 and 3 (1.8 and 2.2 vol.%, respectively) than in alloy 1 (1.2 vol.%).

The TEM experiments reveal that the rectangular or elliptical particles with a length of ~ 100 nm and a width of ~ 40 nm are $Al_{18}Cr_2Mg_3$ and $Al_{20}Mn_3Cu_2$ dispersoids (Fig. 3b) precipitated during heating of the as-cast ingots to the homogenisation temperature. Their spatial distribution is governed by the segregation of the Cr and Mn and corresponds to the former casting dendrites. As expected, significant coarse grain boundary precipitation occurred in all three alloys (Fig. 3c). For a given quench condition, area coverage of the boundaries is relatively high (>0.5). The TEM/EDS

characterisation of precipitation indicates that the chemical compositions of these precipitates having generally ellipsoidal shape (average length is ~ 60 nm and width is ~ 20 nm) are close to formulae of η-$MgZn_2$ phase. These quench-induced precipitates are also present within the grains (Fig. 3b). They are mostly nucleated on dispersoids and reach an average size of ~ 40 nm. These precipitates are coarser than hardening η precipitates developed in the matrix during ageing treatment (Fig. 3). This precipitation occurs homogeneously in the grain interiors associated with the segregation of alloying elements during solidification, so that the grain and dendrite arm boundaries are surrounded by solute-depleted PFZs, whose average width varies between 1.37 and 2.14 μm (see Table 1). This might reflect in the proportion of microvoid initiation within the matrix and a competition process between transgranular and intergranular fracture.

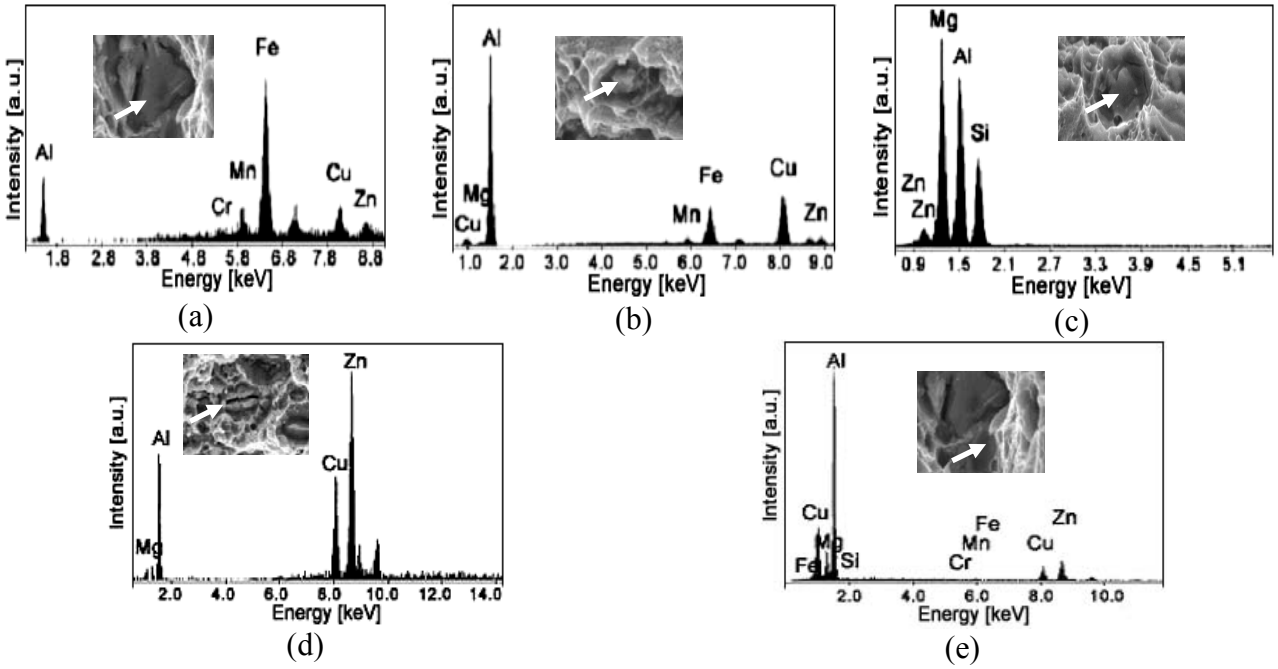

Fig. 2. EDS spectra from coarse particles of $(Cu,Fe,Mn)Al_3$ (a), Al_7Cu_2Fe (b), Mg_2Si (c), η-$Mg(Zn,Cu,Al)_2$ (d) and S-$CuMgAl_2$ (e) phases observed on the fracture surface of broken K_{Ic} specimens.

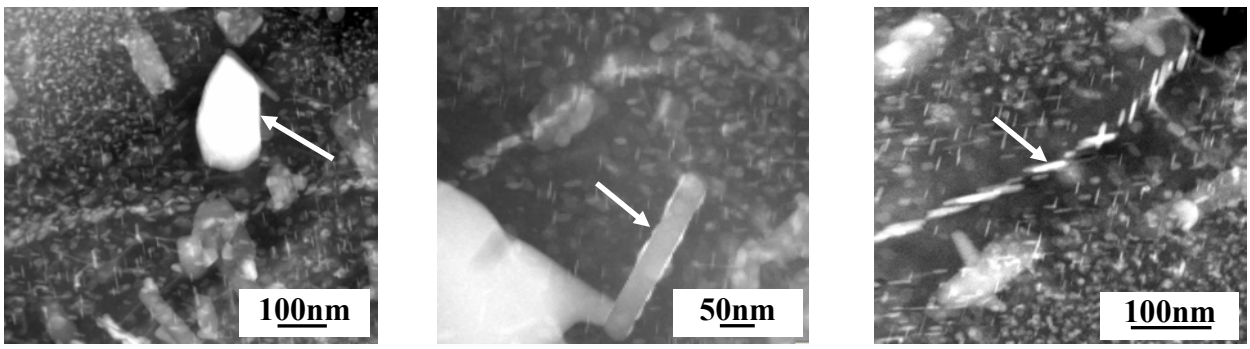

Fig. 3. TEM micrographs showing coarsened intragranular η-$Mg(Zn,Cu,Al)_2$ and S-$CuMgAl_2$ precipitates (a), $Al_{18}Cr_2Mg_3$ and $Al_{20}Mn_3Cu_2$ dispersoids (b), intragranular (b) and intergranular quench-induced η-$MgZn_2$ precipitates (c).

Fracture Modes Observations. This hypothesis is further supported by the fractographic analysis. The presence of ductile areas with numerous microvoids associated with matrix precipitates, large dimples around damaged IM particles (essentially Fe-rich and Mg_2Si) most of which are fractured, flat intergranular areas characterised by a fine population of shallow dimples and ridges at which the crack had changed its propagation direction (Figs. 1b and c) suggests that the fracture process

involves different micromechanisms. Two fracture modes predominate: coarse primary voiding at large IM particles and microvoid-induced transgranular fracture through the grains. The controlling micromechanism varies with alloy purity and specimen orientation.

As can be seen from the area fraction of transgranular fracture (A_{At}) given in Table 2, this fracture mode is most significant in the R-L orientation. The highest proportion of transgranular fracture is encountered in the most pure alloy 1. An increase in the (Fe+Si) content increases the area fraction of coarse voiding (A_{Ap}). But, although the A_{At} decreases from 0.643 to 0.571 as the (Fe+Si) content increases from 0.23 to 0.37 mass%, the fracture is predominantly transgranular. However, in the L-R specimens, where the crack propagation is in the direction which is also the direction along which the coarse IM particles are aligned, coarse voiding becomes more significant. The A_{Ap} increases from 0.152 to 0.378 with the increase of volume fraction of Fe-rich and Mg_2Si particles from 0.352 to 0.737 vol.%, so that a transition from predominantly transgranular fracture to principally coarse voiding occurs in the case of alloy 3.

Table 2. Mechanical tests and quantitative fractography data.

Alloy	***Specimen orientation***	***σ_y [Mpa]***	***K_{Ic} [MPa·m$^{1/2}$]***		***Area fraction of fracture modes***		
			measured	**predicted**	***A_{Ap}***	***A_{Ai}***	***A_{At}***
1	R-L	288	49.8	48.2	0.203±0.013	0.154±0.032	0.643±0.036
	L-R	322	43.2	39.7	0.152±0.016	0.278±0.028	0.570±0.024
2	R-L	283	46.2	40.6	0.240±0.066	0.207±0.039	0.553±0.106
	L-R	310	40.9	35.9	0.299±0.017	0.304±0.022	0.397±0.029
3	R-L	318	44.1	40.4	0.287±0.029	0.142±0.005	0.571±0.035
	L-R	332	37.7	33.0	0.378±0.028	0.287±0.018	0.335±0.036

From the preceding, one would expect that the alloy 1 is more ductile, as compared to both alloys 2 and 3. The tensile and fracture toughness data presented in Table 2 show that the yield strength decreases and the fracture toughness increases on increasing alloy purity. However, all three alloys show higher K_{Ic} values in the R-L orientation as compared to that of the L-R. This is consistent with the fact that the intermediate and fine particles are not found to fracture, so that the transgranular fracture involves significant dissipation of plastic energy. Therefore, the increase in the A_{At} leads to an increase in the K_{Ic}. Contrary, the coarse IM particles fracture and decohesion involve very little plastic energy dissipation, and hence, a fracture dominated by coarse particle cracks in the alloy 3 leads to low toughness. It appears, however, that the main factor determining the difference in fracture toughness between the R-L and L-R orientation is anisotropic orientations of grain and dendrite boundaries apart from the coarse IM particles. When the grain or dendrite boundary segment is oriented favourably, the fracture is more likely to progress through that boundary segment. Although it is often difficult to resolve intergranular fracture mode, its proportion (A_{Ai}) is higher for all alloys in the L-R orientation than in the R-L orientation leading to a further decrease in the fracture toughness.

Modelling. Recognising that the void initiation at the coarse IM particles is the critical step in the fracture process, we used the equation previously established by Hahn and Rosenfield [7] as a starting relation of the new proposed model. Namely, among a number existing models [2-4,7], which are exclusively based on only one scale and seldom constructed to describe the coupling influences of the two types of second-phase particles, only in their model the effect of the volume fraction, f_v, and size, D, of coarse particles was considered. However, this model does not valid, since we have shown that the fracture resistance is controlled by the coarse particle fracture, the plastic properties of the matrix and the grain boundary structure. By including the relevant microstructural parameters and area fraction of main fracture modes in the Hahn and Rosenfield model, the following relationship is derived:

$$K_{Ic} = \left[2 \cdot \sigma_y \cdot E \cdot \left(\frac{\pi}{6} \right)^{1/3} \cdot D \right]^{1/2} \cdot f_v^{-1/6} \cdot A_{Ap}^{-m} \cdot \exp\left[(A_{At})^{1/2} \cdot \exp\left(-\left(\frac{n \cdot w_{PFZs}}{\lambda} \right)^{1/2} \right) \right]. \quad (1)$$

where σ_y is the yield stress, E is Young's modulus, n is a number of PFZs observed between coarse particles distributed over the λ distances and exponent m depends on coarse IM particles fraction (for lower fraction $m \approx 0.3$, for higher fraction $m \approx 0.5$). The new model is validated by the experimental data presented in this article. The predicted K_{Ic} values well represented the tendency of fracture values, but, overall, the agreement may be considered to be resonably satisfactory. This deviation ranges from 1.6 to 5.6 MPa·m$^{1/2}$, as shown in Table 2, representing only 3.2 or 12.5% of given K_{Ic} values. However, the proposed model exhibits better correlation to data for the case of dominant transgranular fracture mode represented in the R-L orientation.

Conclusions

The fracture process in overaged 7000 alloy forgings is multimechanistic: grain and dendrite boundary fracture, transgranular fracture and coarse voiding at large IM particles occur. The volume fraction of coarse Fe- and Si-containing particles, their size and spacing are important, as coarse voiding at these particles becomes more predominant with increasing the impurity level. The complex interactions between the fracture micromechanisms and the variation of parameters with alloy chemistry make the attempts to model fracture toughness difficult. A new modelling approach, incorporating the Hahn and Rosenfield model dealing with quantitative relationship between toughness and coarse IM particle parameters is derived. The proposed micromechanical model successfully predicts the evolution of fracture toughness when changes in relevant microstructural attributes and occurrence of fracture modes are observed.

Acknowledgements

This work was financially supported by the Ministry of Science and Environmental Protection of the Republic of Serbia through the project No. 144027.

References

[1] D. Dumont, A. Deschamps and Y. Bréchet: Mater. Sci. Eng. A Vol. 356 (2003), p. 326
[2] N. Kamp, I. Sinclair and M.J. Starink: Metall. Mater. Trans. A Vol. 33A (2002), p. 1125
[3] B. Morere, J.-C. Ehrstrom, P.J. Gregson and I. Sinclair: Mater. Trans. A Vol. 31A (2000), p. 2503
[4] D. Dumont, A. Deschamps and Y. Bréchet: Acta Mater Vol. 52 (2004), p. 2529
[5] N.U. Deshpande, A.M. Gokhale, D.K. Denzer and J. Liu: Metall. Mater. Trans. A Vol. 29A (1998), p. 1191
[6] G. Patton, C. Rinaldi, Y. Bréchet, G. Lormand and R. Fougéres: Mater. Sci. Eng. A Vol. 254 (1998), p. 207
[7] G.T. Hahn and A.R. Rosenfield: Metall. Trans. A Vol. 6A (1975), p. 653